

Depth-averaged flow models on arbitrarily curved topography

Dieter Issler*

Norwegian Geotechnical Institute, P. O. Box 3930 Ullevål Stadion, 0806 Oslo, Norway

Abstract

For a quite general class of gravity mass flow models we show how to apply well-known methods of differential geometry to formulate the basic balance equations for mass and momentum in a curvilinear coordinate system. This approach does not require the strong assumption that the curvature radius is much larger than the typical flow length scale; it has to be larger than the flow depth, however. We find that the general structure of the depth-averaged balance equations does not change radically: Effects induced by the curvature of the bed surface, such as centrifugal forces, appear mostly as source terms and do not spoil the conservation properties of the balance equations. For several frequently used rheological assumptions, we discuss their formulation in general coordinate systems. In a numerical implementation of such models, flow-depth-dependent geometric factors need to be evaluated at each mesh point and each timestep. For two particular choices of coordinates we determine the metric tensor and the Christoffel symbols and show how to evaluate the geometric factors in an efficient way.

*E-mail: *di@ngi.no*

1 Introduction

Most subaerial and many subaqueous gravity mass flows (GMFs) such as submarine slides, pyroclastic flows, rock avalanches, debris flows and snow avalanches take place in complex topography that strongly influences the path chosen by the flow. For example, small hummocks or shallow stream beds may strongly deflect or channelize the relatively slow dense-flow part of snow avalanches while the dilute, deep suspension layer (“powder snow cloud”) is much less affected and continues along a nearly straight trajectory; similar effects occur in pyroclastic flows and submarine debris flows where dilute suspension layers develop that may follow different trajectories. The dominant, velocity-independent effect of terrain topography on mass flows is the variable strength and direction of the slope-parallel projection of the gravitational force. In addition, terrain curvature leads to centrifugal (pseudo-)forces that increase or diminish the bed-normal stresses and also Coulomb-type frictional forces in dense flows. A comparison of various avalanche flow models on the basis of avalanche measurements from the Norwegian test site at Ryggfonn indicated that the extra friction in bends, e. g. at the foot of a dam, shortens the runout distance by 20–50 m.

Three-dimensional flow simulation codes intrinsically take into account centrifugal forces. However, the vast majority of GMF models in practical use today are depth-averaged codes because they require almost two orders of magnitude less computing resources (memory and time). Consistent derivation of these models from the fundamental equations of fluid mechanics requires either the use of curvilinear coordinates or extra care in the treatment of the out-of-surface dimension. In the first approach, derivatives are replaced by covariant derivatives, which lead to extra terms that are found to contain the centrifugal forces, among others. In practice, most models disregard these effects and only take into account the slope-angle dependence of the down-slope and bed-normal components of the gravitational acceleration.

Probably the first paper including curvature effects is due to [1]. In a series of papers, Hutter and coworkers [2, 3, and references therein] used curvilinear coordinates consistently and developed a scaling analysis for granular gravity mass flows that allowed them

to drop most curvature-related terms in a controlled way. To do so, they assumed the flows to be shallow, with the ratio $\epsilon \equiv H/L$ of the typical flow depth and length or width of order 10^{-2} . Various assumptions can be made for the ratio of the typical path curvature radius R and flow length. Hutter and coworkers assume $L/R \sim \epsilon^{1/2}$ and then are entitled to neglect all curvature effects except the centrifugal force if they keep terms up to order ϵ . However, in many practical cases this ordering may not be fulfilled: Avalanches or debris flows in narrow gullies may be characterized by $\epsilon \sim 0.1$ and $L/R \sim \mathcal{O}(1)$ or even $\mathcal{O}(\epsilon^{-1/2})$. Similarly, avalanches from open slopes may encounter curvature radii of the order of 10–50 m when they hit the bottom of a V-shaped valley.

Therefore our objective is to formulate a general depth-averaged GMF model in curvilinear coordinates adapted to the mountain slope. In order to avoid unnecessary complications, we assume that the surface $z = 0$ coincides with the terrain, that the z -coordinate has a constant scale throughout the considered domain, and that erosion is sufficiently slow and smooth so that the geometric quantities may be considered time-independent. We will show that the resulting expressions, even though necessarily complex, do not strongly affect the structure of the code. However, geometrical coefficients that depend on the flow depth and the vertical profiles of the dynamical fields have to be evaluated at every time step and for every grid point. These computations should therefore be designed to be as efficient as possible.

We shall not address the complex task of creating suitable computational meshes here, but assume that the models use a quadrangular (structured) surface mesh. However, for two particular choices of coordinates that may be of interest in practical applications we elaborate explicit expressions for the metric tensor and the Christoffel symbols. They differ widely in complexity and the effort needed for creating a grid, but also in the expected quality of the meshes. It remains to be seen in the course of model implementation and testing which of these options is preferable.

In order to make this paper accessible to potential model developers and users without extensive theoretical background, the most important issues in depth averaging in a Cartesian coordinate system are reviewed in Sect. 2, and Sect. 3 summarizes the main

concepts from differential geometry used in Sect. 4. Section 5 contains a brief discussion on how to extend some of the popular rheological models to three dimensions so that they can be used in this context. After drawing conclusions from our work, Sect. 6 discusses similarities and differences with recent similar work. For ease of reading, tables of coefficients appearing in the balance equations of mass and momentum are collected in the Appendices A and B for two particular types of coordinate system.

2 Depth-averaging in Cartesian coordinates

This section serves to establish the notation and provide the starting point for the generalization of the conservation equations from Cartesian to curvilinear coordinates. We consider a fairly general system that comprises most models presently in practical use. However, for simplicity, we will limit ourselves to a single moving layer; the extension to multi-layer models is straightforward.

In a Cartesian coordinate system, the local balance laws for the mass and the momentum of a fluid of variable density, ρ , are written in conservative form as^{a)}

$$\partial_t \rho + \partial_J(\rho u^J) = 0, \quad (1)$$

$$\partial_t(\rho u^I) + \partial_J(\rho u^I u^J) = \partial_J(\sigma^{IJ}) + \rho G^I. \quad (2)$$

u^I , σ^{IJ} and G^I are the velocity, stress tensor and gravitational acceleration, respectively. For the latter we use a capital letter to distinguish it from the metric tensor, to be introduced below. We use the Einstein summation convention throughout, i. e., repeated indices are to be summed over unless they are set between parentheses. Note that lower (covariant) and upper (contravariant) indices are distinguished for vector and tensor components in anticipation of the transformation to curvilinear coordinates.

For slender flows over a plane surface at $Z = 0$ it is often sufficient for practical purposes to calculate the mean values of the field variables across the flow depth $h(X, Y, t)$,

^{a)}Partial derivatives with respect to t or x^i are denoted by $\partial_t \equiv \frac{\partial}{\partial t}$ and $\partial_i \equiv \frac{\partial}{\partial x^i}$, respectively. Capital letters for the indices indicate that they refer to a Cartesian coordinate system.

e. g., $\bar{\rho}(X, Y, t) = (1/h(X, Y, t)) \int_b^s \rho(X, Y, Z, t) dZ$ where $b(X, Y, t)$ and $s(X, Y, t)$ are the Z -coordinates of the bed and flow surfaces, respectively, and the flow depth is given by $h(X, Y, t) = s(X, Y, t) - b(X, Y, t)$. The field equations for the depth-averaged fields can be obtained from the local field equations (1) and (2) by integrating them over the Z -direction, taking account of the X and Y dependence of the boundaries when interchanging differentiation and integration. From the mass balance we obtain

$$\begin{aligned} \partial_t(h\bar{\rho}) + \partial_\Gamma(h\bar{\rho}\bar{u}^\Gamma) &= \rho(s)[\partial_t s + u^\Gamma(s)\partial_\Gamma s - u^Z(s)] \\ &\quad - \rho(b)[\partial_t b + u^\Gamma(b)\partial_\Gamma b - u^Z(b)]. \end{aligned} \quad (3)$$

Greek indices run over the in-plane coordinates X and Y only, and the dependence of the fields on X , Y and t has been suppressed for easier reading. On the right-hand side, the terms in square brackets are due to the variability of the integration limits and the integration of $\partial_Z(\rho u^Z)$ over Z . Kinematic boundary conditions apply at both boundaries:

$$\begin{aligned} \rho(s^-) [\partial_t s + u^X(s^-)\partial_X s - u^Z(s^-)] \\ = \rho(s^+) [\partial_t s + u^X(s^+)\partial_X s - u^Z(s^+)] \equiv q_s. \end{aligned} \quad (4)$$

$$\begin{aligned} \rho(b^+) [\partial_t b + u^X(b^+)\partial_X b - u^Z(b^+)] \\ = \rho(b^-) [\partial_t b + u^X(b^-)\partial_X b - u^Z(b^-)] \equiv -q_b. \end{aligned} \quad (5)$$

q_s and q_b are the net entrainment rates at the top and bottom surface, respectively; superscript signs indicate whether an interface is to be approached from above (+) or below (-). So we finally arrive at

$$\partial_t(h\bar{\rho}) + \partial_\Gamma(h\bar{\rho}\bar{u}^\Gamma) = q_b + q_s. \quad (6)$$

\bar{u}^Γ is the density-weighted (Favre) average of the velocity:

$$\bar{u}^\Gamma := \frac{h\overline{\rho u^\Gamma}}{h\bar{\rho}} = \frac{\int_b^s \rho(Z)u^\Gamma(Z) dZ}{\int_b^s \rho(Z) dZ}. \quad (7)$$

The depth integration of the momentum balance is carried out along the same lines and yields

$$\begin{aligned} & \partial_t(h\bar{\rho}\bar{u}^I) + \partial_\Lambda \int_b^s \rho u^I u^\Lambda dZ \\ &= h\bar{\rho}G^I + \partial_\Lambda(h\bar{\sigma}^{I\Lambda}) + \rho(s)u^I(s)q_s + \rho(b)u^I(b)q_b \\ &+ \left(\sigma^{IZ}(s) - \sigma^{I\Lambda}(s)\partial_\Lambda s\right) - \left(\sigma^{IZ}(b) - \sigma^{I\Lambda}(b)\partial_\Lambda b\right). \end{aligned} \quad (8)$$

The second term on the left-hand side can be expressed in terms of averaged fields as

$$\int_b^s \rho u^I u^J dZ = d_u \bar{\rho} \bar{u}^I \bar{u}^J, \quad (9)$$

where the Boussinesq coefficients are defined by

$$d_u = \frac{\left(\int_b^s \rho dZ\right) \left(\int_b^s \rho u^I u^J dZ\right)}{\left(\int_b^s \rho u^{(I)} dZ\right) \left(\int_b^s \rho u^{(J)} dZ\right)} \quad (10)$$

and the notation d_u anticipates an extra assumption that makes them the same for all tensor components, see below. To evaluate them, one assumes that the velocity profile has approximately the same shape everywhere in space and time, and similarly for the density, i. e.,

$$\rho(X, Y, Z, t) \approx f_\rho(\zeta) \bar{\rho}(X, Y, t), \quad (11)$$

$$u^I(X, Y, Z, t) \approx f_u(\zeta) \bar{u}^I(X, Y, t), \quad (12)$$

where $\zeta \equiv (Z - b)/h$, $0 \leq \zeta \leq 1$ and it has been assumed that the shape of the velocity profile is the same for both tangential components. The following normalization conditions are imposed:

$$\int_0^1 f_\rho(\zeta) d\zeta = 1, \quad \int_0^1 f_\rho(\zeta) f_u(\zeta) d\zeta = 1. \quad (13)$$

Later on, the vertical profiles of the stresses will also be needed:

$$\sigma^{IJ}(X, Y, Z, t) \approx f_\sigma(\zeta) \bar{\sigma}^{IJ}(X, Y, t), \quad (14)$$

with

$$\int_0^1 f_\sigma(\zeta) d\zeta = 1. \quad (15)$$

Equation (8) simplifies considerably if the upper surface is assumed to be stress-free and material ($q_s = 0$), if the material entrained at the bottom enters the flow at zero velocity, and if $\partial_\Lambda b$ can be neglected. With these approximations, the momentum balance finally takes the form

$$\partial_t(h\bar{\rho}\bar{u}^I) + \partial_\Lambda(d_u\bar{\rho}\bar{u}^I\bar{u}^\Lambda) = h\bar{\rho}G^I + \partial_\Lambda(h\bar{\sigma}^{I\Lambda}) - \sigma_b^{IZ}. \quad (16)$$

Subscripts b and s will from now on denote quantities evaluated at the bed and the upper surface, respectively.

3 Curvilinear coordinate systems

3.1 Basic notions of differential geometry

We are concerned here with a curved two-dimensional surface (the terrain) embedded in flat Euclidean three-dimensional space. Thus, the metric tensor in space can be obtained from the unit tensor by means of a coordinate transformation. Before we apply depth averaging, we work in a 3D space bounded by a curved (2D) surface. After depth averaging, no more explicit reference is made to the 3D space and we have to deal with a theory on an intrinsically curved 2D manifold. This means that the 2D metric tensor cannot be obtained from the 2D unit tensor by a coordinate transformation.

A fundamental role is played by the three tangent vectors (the so-called local frame) $\mathbf{e}_i(\mathbf{r}) = \partial\mathbf{r}/\partial x^i$ to the (curvilinear) coordinate lines x^i , $i = 1, 2, 3$, at each point \mathbf{r} in space^{b)}. The metric tensor is obtained from the scalar products of the local frame:

$$g_{ij}(\mathbf{r}) = \mathbf{e}_i(\mathbf{r}) \cdot \mathbf{e}_j(\mathbf{r}). \quad (17)$$

^{b)}In order to clearly distinguish (the location of) a space point from the coordinates, we designate the space location by \mathbf{r} and the coordinates by x^i here.

Under coordinate transformations, $x^i = x^i(x'^j)$, the local frame transforms covariantly according to

$$\mathbf{e}_i(\mathbf{r}) = \frac{\partial \mathbf{r}}{\partial x^i} = \frac{\partial \mathbf{r}}{\partial x'^j} \frac{\partial x'^j}{\partial x^i} = \mathbf{e}'_j \frac{\partial x'^j}{\partial x^i}. \quad (18)$$

Since a vector $\mathbf{v}(\mathbf{r}) \equiv v^i(\mathbf{r})\mathbf{e}_i(\mathbf{r}) \equiv v'^j(\mathbf{r})\mathbf{e}'_j(\mathbf{r})$ is unchanged under coordinate transformations, its contravariant components transform as

$$v^i(\mathbf{r}) = v'^j(\mathbf{r}) \frac{\partial x^i}{\partial x'^j}(\mathbf{r}). \quad (19)$$

In tensors, each covariant (lower-index) component transforms according to (18) and each contravariant (upper-index) one according to (19).

The change of a scalar-valued function $f(\mathbf{r})$ between two infinitesimally distant points \mathbf{r} and $\mathbf{r} + d\mathbf{r}$ is calculated in a curvilinear coordinate system as in the Cartesian case: $df \equiv f(\mathbf{r} + d\mathbf{r}) - f(\mathbf{r}) = \partial_i f(\mathbf{r}) dx^i$. However, the components of a vector or tensor-valued function refer to different local frames at the two points, thus one finds

$$\begin{aligned} d\mathbf{v}(\mathbf{r}) &\equiv \mathbf{v}(\mathbf{r} + d\mathbf{r}) - \mathbf{v}(\mathbf{r}) \\ &= v^i(\mathbf{r} + d\mathbf{r})\mathbf{e}_i(\mathbf{r} + d\mathbf{r}) - v^i(\mathbf{r})\mathbf{e}_i(\mathbf{r}) \\ &= [v^i(\mathbf{r}) + \partial_j v^i(\mathbf{r}) dx^j][\mathbf{e}_i(\mathbf{r}) + \partial_k \mathbf{e}_i(\mathbf{r}) dx^k] - v^i(\mathbf{r})\mathbf{e}_i(\mathbf{r}) \\ &= \partial_j v^i(\mathbf{r})\mathbf{e}_i(\mathbf{r}) dx^j + v^i(\mathbf{r})\partial_j \mathbf{e}_i(\mathbf{r}) dx^j. \end{aligned} \quad (20)$$

Since the $\mathbf{e}_i(\mathbf{r})$ span the local tangent space at \mathbf{r} , their derivatives must be expressible as linear combinations of the \mathbf{e}_i :

$$\partial_j \mathbf{e}_i(\mathbf{r}) = \partial_i \partial_j \mathbf{r} = \Gamma_{ij}^k(\mathbf{r})\mathbf{e}_k(\mathbf{r}). \quad (21)$$

The connection coefficients (or Christoffel symbols) $\Gamma_{ij}^k(\mathbf{r})$ are thus symmetric with respect to their two lower indices. They can be computed from the metric tensor, g_{ij} , and its inverse, g^{ij} , by suitably permuting indices in (21) and combining the resulting expressions:

$$\Gamma_{ik}^j \equiv \frac{1}{2} g^{jl} (\partial_k g_{il} + \partial_i g_{kl} - \partial_l g_{ik}). \quad (22)$$

The covariant derivative of (the contravariant components of) a vector is defined through the relation

$$\mathcal{D}_i v^j \equiv (\delta_k^j \partial_i + \Gamma_{ik}^j) v^k, \quad (23)$$

where the Kronecker delta is 1 if both indices are equal and 0 otherwise. Proceeding in the same way for a second-rank tensor, one gets

$$\mathcal{D}_k T^{ij} = (\delta_m^i \delta_n^j \partial_k + \delta_n^j \Gamma_{km}^i + \delta_m^i \Gamma_{kn}^j) T^{mn} \quad (24)$$

The covariant derivative of the covariant components of a vector turns out to be

$$\mathcal{D}_i v_j = (\delta_j^k \partial_i - \Gamma_{ij}^k) v_k. \quad (25)$$

An infinitesimal volume element in the curvilinear system is spanned by the local frame $\{\mathbf{e}_1(\mathbf{r}), \mathbf{e}_2(\mathbf{r}), \mathbf{e}_3(\mathbf{r})\}$; its volume is

$$\begin{aligned} dV &= \mathbf{e}_1 \cdot (\mathbf{e}_2 \times \mathbf{e}_3) dx^1 dx^2 dx^3 \\ &= \sqrt{\det(g_{ij})} d^3x \equiv \sqrt{g(\mathbf{r})} d^3x. \end{aligned} \quad (26)$$

The covariant divergence of a vector can be shown to be

$$\mathcal{D}_i v^i = \delta_i^j \mathcal{D}_j v^i = \frac{1}{\sqrt{g}} \partial_i (\sqrt{g} v^i). \quad (27)$$

Finally, the covariant divergence of a symmetric second-rank tensor $S^{ij} = S^{ji}$ will be needed (e. g., for the stress tensor σ^{ij}):

$$\begin{aligned} \mathcal{D}_j S^{ij} &= \partial_j S^{ij} + \Gamma_{jk}^i S^{kj} + \Gamma_{jk}^j S^{ik} \\ &= \frac{1}{\sqrt{g}} \partial_j (\sqrt{g} S^{ij}) + \Gamma_{jk}^i S^{jk}. \end{aligned} \quad (28)$$

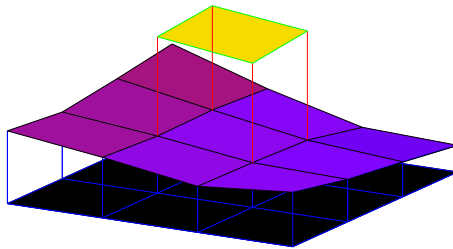


Figure 1: Schematic representation of the coordinate system obtained by vertically projecting a regular grid in the X - Y -plane onto the bed surface and extending it into space along a fixed z -direction (coinciding with the Z -direction in the figure). Only one cell of the flow is shown.

3.2 Physical vs. covariant vector and tensor components

Among the dynamical variables of the model, the density ρ is a scalar, the gravitational acceleration $\mathbf{G} = \check{G}^i \mathbf{e}_i$ and the velocity $\mathbf{u} = \check{u}^i \mathbf{e}_i$ are vectors whereas the stress $\sigma = \check{\sigma}^{ij} \mathbf{e}_i \mathbf{e}_j$ is a symmetric second-rank tensor. There is a small but important point to notice: Contravariant vector and tensor components transform in the same way as differentials; they measure the size of the vector (or tensor) in a specific direction in terms of the *local, direction-dependent* “ruler” specified by corresponding local frame vector \mathbf{e}_i or, equivalently, the metric. Thus, a velocity component of 17 i -units per second at a given location will not usually be the same *physical* velocity as 17 j or k -units per second at the same point, nor will it be the same as 17 i -units per second at another location. However, when specifying initial conditions and material properties or analyzing simulation results, we have to use physical components G^i , u^i , σ^{ij} defined by

$$\begin{aligned}
 G^i &= \sqrt{g^{(ii)}} \check{G}^i & G_i &= \sqrt{g^{(ii)}} \check{G}_i \\
 u^i &= \sqrt{g^{(ii)}} \check{u}^i & \text{or} & & u_i &= \sqrt{g^{(ii)}} \check{u}_i \\
 \sigma^{ij} &= \sqrt{g^{(ii)}g^{(jj)}} \check{\sigma}^{ij} & \sigma_{ij} &= \sqrt{g^{(ii)}g^{(jj)}} \check{\sigma}_{ij}.
 \end{aligned} \tag{29}$$

The parentheses around the repeated indices indicate that no summation is implied. Note that *neither* G^i , u^i , σ^{ij} *nor* G_i , u_i , σ_{ij} *transform as tensors*.

3.3 Particular coordinate systems

Before proceeding to depth-integrate the balance equations, we briefly consider the simplifications afforded by special coordinate systems. g_{ij} can be made independent of z if S_z is obtained by translating S_0 by the distance z along a fixed direction \mathbf{n} , independent of x and y . Considering that topographical (or bathymetric) data is most often available as altitude (depth) values $Z_{m,n} = Z(X_m, Y_n)$ over a horizontal rectangular grid in the X - Y plane with constant mesh widths ΔX , ΔY , we let the coordinate lines $y = \text{cst.}$ and $x = \text{cst.}$ be the intersections of the X - Z and Y - Z planes with S_0 , see Fig. 1. The orientation of the tangent plane at a point on S_0 can be characterized by the inclination angles $\theta_{x,y}$ in the X and Y -directions, respectively. The metric tensor takes the form

$$(g_{ij}) = \begin{pmatrix} 1 + \tan^2 \theta_x & \tan \theta_x \tan \theta_y & \tan \theta_x \\ \tan \theta_x \tan \theta_y & 1 + \tan^2 \theta_y & \tan \theta_y \\ \tan \theta_x & \tan \theta_y & 1 \end{pmatrix} \quad (30)$$

and has unit determinant. The corresponding connection coefficients are listed in Appendix A.

Another simplifying choice is to set the z -direction everywhere perpendicular to the bed surface, with constant scale along that direction. The metric tensor then has the form

$$(g_{ij}) = \begin{pmatrix} g_{11} & g_{12} & 0 \\ g_{21} & g_{22} & 0 \\ 0 & 0 & 1 \end{pmatrix}, \quad (31)$$

where the four components g_{11} , $g_{12} = g_{21}$ and g_{22} depend on $x \equiv x^1$, $y \equiv x^2$ and $z \equiv x^3$. The surfaces $z = \text{cst.}$ are parallel to the bed in the sense that the tangent plane at (x_0, y_0, z) is parallel to the tangent plane at $(x_0, y_0, 0)$. Given the metric tensor $g_{ij}(x, y, 0)$, what is $g_{ij}(x, y, z)$?

Let the bed surface S_0 be described by the points $\mathbf{r}_0(x, y)$. A family of parallel surfaces S_z , $0 \leq z < R_{\min}$ (R_{\min} being the minimum radius of curvature in S_0) is defined with the

help of the unit normal vectors \mathbf{n} on S_0 :

$$\mathbf{r}(x, y, z) = \mathbf{r}_0(x, y) + z\mathbf{n}(x, y). \quad (32)$$

The metric tensor in a point on S_z can be expressed as

$$g_{ij}(x, y, z) = \partial_i \mathbf{r}(x, y, z) \cdot \partial_j \mathbf{r}(x, y, z). \quad (33)$$

We obtain the tangent vectors to the coordinate directions:

$$\mathbf{e}_i(x, y, z) = \partial_i [\mathbf{r}_0(x, y) + z\mathbf{n}(x, y)] \quad (34)$$

$$= (1 - \delta_{i3})[\partial_i \mathbf{r}_0(x, y) + z\partial_i \mathbf{n}(x, y)] + \delta_{i3}\mathbf{n}(x, y). \quad (35)$$

With $\mathbf{e}_\alpha^{(0)} \equiv \partial_\alpha \mathbf{r}_0(x, y)$, $\alpha = 1, 2$, the partial derivatives of the unit normal vector are expressible as $\partial_\alpha \mathbf{n}(x, y) = c_\alpha^\beta(x, y)\mathbf{e}_\beta^{(0)}(x, y)$ and $\partial_z \mathbf{n}(x, y) = 0$. If the metric tensor on S_0 is written as

$$\begin{aligned} g_{ij}^{(0)}(x, y) &= g_{ij}(x, y, 0) \\ &= (1 - \delta_{i3})(1 - \delta_{j3})\mathbf{e}_i^{(0)}(x, y) \cdot \mathbf{e}_j^{(0)}(x, y) + \delta_{i3}\delta_{j3}, \end{aligned} \quad (36)$$

the metric tensor away from the bed surface takes the form

$$\begin{aligned} g_{ij}(x, y, z) &= g_{ij}^{(0)}(x, y) + (1 - \delta_{i3})(1 - \delta_{j3}) \times \\ &\quad \times \left(z c_j^k g_{ik}^{(0)} + z c_i^k g_{jk}^{(0)} + z^2 c_i^k c_j^k g_{jk}^{(0)} \right). \end{aligned} \quad (37)$$

If we choose orthogonal coordinates on S_0 so that the metric tensor is diagonal, Equation (37) shows that this property is not generally preserved above S_0 : The 2×2 -matrix c_α^β has to be diagonal as well, implying that c_1^1 and c_2^2 are the negative curvatures $-\kappa_{1,2}$ of normal sections of S_0 . Thus we may write $d\mathbf{n} = -\kappa_{1,2}d\mathbf{r}$. Rodrigues' theorem then leads to the conclusion that such coordinate lines are curvature lines and $\kappa_{1,2}$ are indeed

the principal curvatures on S_0 . In this case, the metric tensor takes the explicit form

$$(g_{ij}) = \begin{pmatrix} A^2(1 - \kappa_1 z)^2 & 0 & 0 \\ 0 & B^2(1 - \kappa_2 z)^2 & 0 \\ 0 & 0 & 1 \end{pmatrix}. \quad (38)$$

$A(x, y)$ and $B(x, y)$ are two functions on the bed surface that describe the spatial dependence of the length scales in the x and y -directions. In these coordinates, almost half of the Christoffel symbols vanish identically, see Appendix B for the explicit expressions for the Γ_{jk}^i . It is furthermore possible to assign $y = 0$ to one x -line, e.g. the thalweg, and to impose $A(x, 0) \equiv 1$ along this line. Similarly, $B(x_0, y) \equiv 1$ can be imposed along one selected y -line.

3.4 Computation of geometric quantities from a digital terrain model

In practical applications of GMF models, the terrain is given by a digital terrain model (DTM), usually in the form of a regular grid of altitude values. The task of reading these values, interpolating them as necessary to set the nodes of the mesh, computing all the required geometrical information, and passing it to the flow code in an appropriately formatted file will usually be assigned to a separate grid generator program. The flow solver code needs information on the topology (i.e., which cells touch a given cell), on the side lengths of the cells, their inclination, the curvature along the coordinate lines and the Christoffel symbols. In addition, the initial conditions for the flow at each grid node (typically the release height, the depth of entrainable bed material and the physical properties of the flow and bed material, such as density, yield strength, friction parameters, etc.) have to be set after suitable interpolation. Grid generation has become a computational discipline in its own, and even an elementary treatment of this topic is far beyond the scope of this paper. We limit ourselves to outlining the basic steps of a method for constructing a coordinate system consisting of curvature lines from a DTM.

In the first step, the basis vectors forming the local frame are approximated using the

node points. Assume a regular quadrangular grid with cell edges along the coordinate lines $x = x^1 = \text{cst.}$ and $y = x^2 = \text{cst.}$, respectively, and nodes labeled by (m, n) , where the integers m, n are at the same time the node coordinates in “computational” space. The local frame may be defined by the relations

$$\begin{aligned}\mathbf{e}_1(\mathbf{r}_{m,n}) &= \frac{1}{2}(\mathbf{r}_{m+1,n} - \mathbf{r}_{m-1,n}), \\ \mathbf{e}_2(\mathbf{r}_{m,n}) &= \frac{1}{2}(\mathbf{r}_{m,n+1} - \mathbf{r}_{m,n-1}), \\ \mathbf{e}_3(\mathbf{r}_{m,n}) &= \frac{\mathbf{e}_1(\mathbf{r}_{m,n}) \times \mathbf{e}_2(\mathbf{r}_{m,n})}{|\mathbf{e}_1(\mathbf{r}_{m,n}) \times \mathbf{e}_2(\mathbf{r}_{m,n})|}.\end{aligned}\tag{39}$$

With the help of \mathbf{e}_3 , the coordinate system can be extended into space according to Eq. (32). This immediately allows calculation of the metric tensor and its determinant at the grid points according to Eq. (17). Calculation of the connection coefficients requires an additional finite differencing step. If changes of the metric due to erosion or deposition of bed material are neglected, all geometrical information can be computed before the flow simulation and stored in memory.

The second step approximates the derivatives $\partial_\alpha \partial_\beta \mathbf{r}$ with $\alpha, \beta \in \{x, y\}$ again by finite differences and obtains the coefficients $L_{\alpha\beta} = \mathbf{n} \cdot \partial_\alpha \mathbf{e}_\beta$ of the Second Fundamental Form of S_0 at the grid nodes. In the third step, the principal curvatures $\kappa_{1,2}$ at the grid nodes are computed from the equation

$$\kappa^2 g - \kappa(g_{11}L_{22} - 2g_{12}L_{12} + g_{22}L_{11}) + \det L_{\alpha\beta} = 0.\tag{40}$$

In step four, we insert κ_1 and κ_2 in the linear system

$$\begin{cases} (L_{11} - \kappa_a g_{11})x' + (L_{12} - \kappa_a g_{12})y' = 0, \\ (L_{12} - \kappa_a g_{12})x' + (L_{22} - \kappa_a g_{22})y' = 0, \end{cases}\tag{41}$$

for each node. Non-trivial solutions (x'_1, y'_1) and (x'_2, y'_2) are found that are the directions of the curvature lines corresponding to the principal curvatures. The fifth step interpolates the principal curvatures and corresponding directions between grid nodes. Linear

interpolation should be sufficient, but higher-order spline interpolation may give smoother results. In this way, two continuous and mutually orthogonal direction fields are obtained on S_0 .

In the sixth step, the curvature lines are found by numerically integrating the ordinary differential equations characterized by these direction fields. One may begin, e.g., at a point on a thalweg and evolve the coordinate line $\eta = 0$ from there, setting grid points at the desired characteristic grid spacing (the grid spacing is not uniform in such a coordinate system). Then one of these grid points is singled out and the orthogonal coordinate line $\xi = 0$ is computed analogously. Next the lines $\eta = n\Delta\eta$ and $\xi = m\Delta\xi$ are obtained, starting from the corresponding grid point on $\xi = 0$ or $\eta = 0$. The intersections of these lines mark all the grid points (m, n) . Their locations are expressed in terms of the original three-dimensional Cartesian coordinate system. In the last step, the metric tensor and the Christoffel symbols are computed in terms of the new (ξ, η) coordinates.

4 Depth averaging in curvilinear coordinates

4.1 3D equations in curvilinear coordinates

The balance equations for mass and momentum in their usual formulation do not transform as a scalar and a vector, respectively, under a general change of coordinates. The reason is that the ordinary derivative of a vector is not a second-rank tensor. However, if ordinary derivatives are replaced by covariant ones, the modified balance equations transform consistently as a scalar and a vector, respectively, and reduce to the original equations if the coordinate system is Cartesian. The three-dimensional balance equations for mass and momentum now read

$$\partial_t \rho + \frac{1}{\sqrt{g}} \partial_i (\sqrt{g} \rho \check{u}^i) = 0, \quad (42)$$

$$\partial_t (\rho \check{u}^i) + \frac{1}{\sqrt{g}} \partial_j (\sqrt{g} \rho \check{u}^i \check{u}^j) + \Gamma_{jk}^i \rho \check{u}^j \check{u}^k$$

$$= \frac{1}{\sqrt{g}} \partial_j (\sqrt{g} \check{\sigma}^{ij}) + \Gamma_{jk}^i \check{\sigma}^{jk} + \rho \check{G}^i. \quad (43)$$

As we disregard the effect of erosion on the geometry, the factor $\sqrt{g(\mathbf{x})}$ is constant in time at each location. If we multiply these equations by it, they immediately take on their (apparently) conservative form, i. e., the flux terms appear as a pure divergence:

$$\partial_t (\sqrt{g} \rho) + \partial_i (\sqrt{g} \rho \check{u}^i) = 0, \quad (44)$$

$$\begin{aligned} & \partial_t (\sqrt{g} \rho \check{u}^i) + \partial_j (\sqrt{g} (\rho \check{u}^i \check{u}^j - \check{\sigma}^{ij})) \\ &= \sqrt{g} \rho \check{G}^i - \Gamma_{jk}^i \sqrt{g} (\rho \check{u}^j \check{u}^k - \check{\sigma}^{jk}). \end{aligned} \quad (45)$$

Note that the terms containing Christoffel symbols have the structure of source terms.

4.2 Depth integration

We start with the mass balance equation (44) and integrate it along z from the bed at $b(x, y, t)$ to the flow surface at $s(x, y, t)$, interchanging the derivatives and the integral:

$$\begin{aligned} & \partial_t \int_b^s \sqrt{g} \rho dz + \partial_\alpha \int_b^s \sqrt{g} \rho \check{u}^\alpha dz \\ &= - \left[\sqrt{g(z)} \rho(z) (u^z(z) - \partial_t z - \check{u}^\alpha(z) \partial_\alpha z) \right]_b^s. \end{aligned} \quad (46)$$

Quantities evaluated at the bed or the upper flow surface carry the subscript indices b or s , respectively. The index $\alpha = 1, 2$ stands for the velocity components parallel to the terrain surface. The terms generated by the interchange of the derivatives and the integral combine with the boundary terms from the z -component of the divergence to expressions that may be identified with the entrainment rate from the bed and the suspension rate into the ambient fluid, respectively [4].

If we define weighted averages^{c)} by

$$\sqrt{\bar{g}(x, y, t)} = \frac{1}{h(x, y, t)} \int_b^s \sqrt{g(x, y, z)} dz, \quad (47)$$

$$\begin{aligned} \bar{\rho}(x, y, t) &= \frac{1}{h(x, y, t) \sqrt{\bar{g}(x, y, t)}} \times \\ &\times \int_b^s \sqrt{g(x, y, z)} \rho(x, y, z, t) dz, \end{aligned} \quad (48)$$

$$\begin{aligned} \bar{u}^\alpha(x, y, t) &= \frac{1}{h(x, y, t) \sqrt{\bar{g}(x, y, t)} \bar{\rho}(x, y, t)} \times \\ &\times \int_b^s \sqrt{g(x, y, z)} \rho(x, y, z, t) \check{u}^\alpha(x, y, z, t) dz \end{aligned} \quad (49)$$

and the entrainment rate at the bottom and the suspension rate at the top surface,

$$\begin{aligned} q_b(x, y, t) &= \rho_b(x, y, t) u_b^z(x, y, t) - \partial_t b - \check{u}_b^\alpha \partial_\alpha b, \\ q_s(x, y, t) &= \rho_s(x, y, t) u_s^z(x, y, t) - \partial_t s - \check{u}_s^\alpha \partial_\alpha s, \end{aligned} \quad (50)$$

the mass-balance equation can be written in the form

$$\partial_t (\sqrt{\bar{g}} h \bar{\rho}) + \partial_\alpha (\sqrt{\bar{g}} h \bar{\rho} \bar{u}^\alpha) = \sqrt{g_b} q_e - \sqrt{g_s} q_s. \quad (51)$$

The factor $\sqrt{\bar{g}}$ captures the fact that flow “slices” are no longer prisms if there is surface curvature; as (47) shows, $h\sqrt{\bar{g}}$ is the volume of such a slice. Similarly, the factor $\sqrt{g_b}$ appearing with q_e expresses the dependence of the mass growth on the entrainment rate per unit area *and* the area of the bed surface element. (Due to our choice of a coordinate system with $g_{iz} = \delta_{iz}$, $\sqrt{g_b}$ is both the content of the volume element and the area of the surface element at the bed.)

^{c)}The dependence on the parameters is spelled out explicitly in this formula. Throughout the rest of the paper, abbreviated notation will be used where no confusion is expected to arise. As earlier, $x^1 \equiv x, x^2 \equiv y$.

We proceed analogously for the momentum balance and obtain

$$\begin{aligned}
& \partial_t \left(\sqrt{\bar{g}h} \bar{\rho} \bar{u}^i \right) + \partial_\alpha \left[\sqrt{\bar{g}h} \left(b_{(i\alpha)} \bar{\rho} \bar{u}^i \bar{u}^\alpha - \bar{\sigma}^{i\alpha} \right) \right] \\
&= \sqrt{\bar{g}_s} \left(\check{\sigma}_s^{iz} - \check{\sigma}_s^{i\alpha} \partial_\alpha s \right) - \sqrt{\bar{g}_b} \left(\check{\sigma}_b^{iz} - \check{\sigma}_b^{i\alpha} \partial_\alpha b \right) \\
&+ \sqrt{\bar{g}h} \bar{\rho} \check{G}^i - \sqrt{\bar{g}_s} q_s \check{u}_s^i + \sqrt{\bar{g}_b} q_b \check{u}_b^i \\
&- \sqrt{\bar{g}h} \bar{\Gamma}_{jk}^i \left[b_{(i,jk)}^{(1)} \bar{\rho} \bar{u}^j \bar{u}^k - b_{(i,jk)}^{(2)} \bar{\sigma}^{jk} \right] dz.
\end{aligned} \tag{52}$$

Further weighted averages were defined as

$$\bar{\sigma}^{ij} = \frac{1}{\sqrt{\bar{g}h}} \int_b^s \sqrt{g(z)} \check{\sigma}^{ij}(z) dz, \tag{53}$$

$$\check{G}^i = \frac{1}{\sqrt{\bar{g}h} \bar{\rho}} \int_b^s \sqrt{g(z)} \rho(z) \check{G}^i(z) dz, \tag{54}$$

$$\bar{\Gamma}_{jk}^i = \frac{1}{\sqrt{\bar{g}h}} \int_b^s \sqrt{g(z)} \Gamma_{jk}^i(z) dz. \tag{55}$$

Boussinesq coefficients have to be introduced not only for the advective momentum flux but also for the terms containing connection coefficients:

$$b_{ij} = \frac{\left(\int_b^s \sqrt{\bar{g}} \rho \check{u}^i \check{u}^j dz \right) \left(\int_b^s \sqrt{\bar{g}} \rho dz' \right)}{\left(\int_b^s \sqrt{\bar{g}} \rho \check{u}^{(i)} dz'' \right) \left(\int_b^s \sqrt{\bar{g}} \rho \check{u}^{(j)} dz''' \right)} \tag{56}$$

$$\begin{aligned}
b_{(i,jk)}^{(1)} &= \frac{\left(\int_b^s \sqrt{\bar{g}} \Gamma_{jk}^i \rho \check{u}^{(i)} \check{u}^{(j)} dz_1 \right) \left(\int_b^s \sqrt{\bar{g}} \rho dz_2 \right)}{\left(\int_b^s \sqrt{\bar{g}} \rho \check{u}^{(j)} dz_3 \right) \left(\int_b^s \sqrt{\bar{g}} \rho \check{u}^{(k)} dz_4 \right)} \times \\
&\times \frac{\int_b^s \sqrt{\bar{g}} dz_5}{\int_b^s \sqrt{\bar{g}} \Gamma_{(jk)}^{(i)} dz_6}
\end{aligned} \tag{57}$$

$$b_{(i,jk)}^{(2)} = \frac{\left(\int_b^s \sqrt{\bar{g}} \Gamma_{jk}^i \check{\sigma}^{(jk)} dz \right) \left(\int_b^s \sqrt{\bar{g}} dz' \right)}{\left(\int_b^s \sqrt{\bar{g}} \Gamma_{(jk)}^{(i)} dz'' \right) \left(\int_b^s \sqrt{\bar{g}} \check{\sigma}^{(jk)} dz''' \right)} \tag{58}$$

Note that they do not transform as tensors. As discussed in Section 2, these expressions become meaningful only when vertical profile functions $f_\rho(\zeta)$, $f_u(\zeta)$ and $f_\sigma(\zeta)$ are specified for the fields so that the integrals can be evaluated approximately without solving the entire flow problem first. The z -dependence of \sqrt{g} and Γ_{jk}^i is determined by the geometry

of the bed surface and the choice of coordinate system, as discussed in Section 3.3. The next section will consider how to compute these coefficients in practice.

The first main result from Eqs. (51) and (52) is that the depth-integrated balance laws of mass and momentum can be written in explicit conservation form, which is important for numerical models that are to render shock phenomena. The distortion of the volume and surface elements is captured by the ubiquitous factors \sqrt{g} and $\sqrt{g_b}$ or $\sqrt{g_s}$, respectively. Additional effects of terrain curvature are embodied in (depth-integrated) source terms proportional to the connection coefficients.

The first three lines of Eq. (52) contain the terms that also appear in a Cartesian coordinate system when the bed and top surface are inclined relative to the x - y coordinate plane. They are modified only for the curvature effects on the volume of flow slices and on the spatial weighting embodied in the Boussinesq coefficients. The first term in brackets on the second line vanishes if one assumes a stress-free upper flow surface. The last term on the third line vanishes for the tangential components x , y if there is no slip ($\tilde{u}_b^x = 0$). This term vanishes altogether if the bed material is at rest when it is eroded so that the flow gains no momentum by entraining bed material [4, 5]. We will ignore both the entrainment and the suspension terms in the following. The last line represents further curvature effects, which are schematically explained in Fig. 2 for the 2D case. The first term in the bracket reduces to the centrifugal pseudo-force for the z -component, proportional to the curvature and the velocity squared. The longitudinal stresses σ^{xx} and σ^{yy} also contribute to the bed-normal stress because their direction of action at both ends of an infinitesimal volume element is different from the bed-parallel direction at the center section of the element. Similarly, the shear stresses σ^{zx} and σ^{zy} acting at the faces of the volume element have longitudinal components relative to the local frame at the center section.

The centrifugal force, which may give rise to additional or reduced friction in bends, has been included in a variety of published models, but the additional normal force from the longitudinal stresses and longitudinal force from the shear stresses seems to have been neglected in all models known to us. With the exception of [1, 2, 3] and related

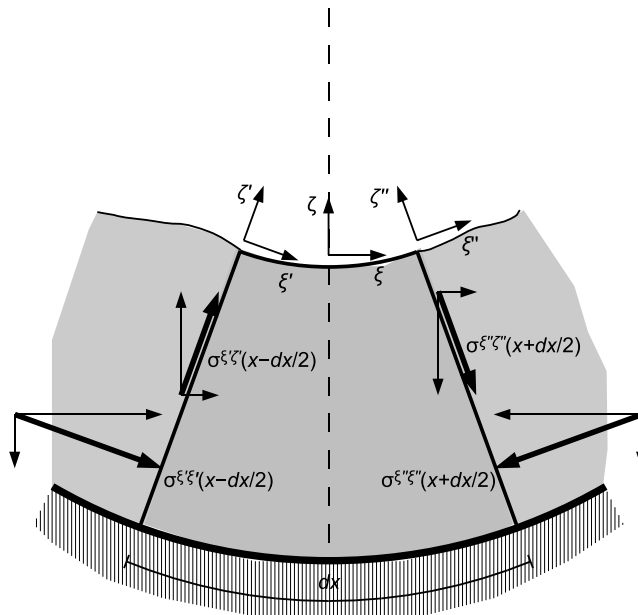


Figure 2: Longitudinal section of flow, showing the forces acting on an (infinitesimal) slice. The local reference frames at the center (x - z), the rear (x' - z') and the front (x'' - z'') are indicated. It is seen that $\sigma_{x'z'}(x - dx/2)$ and $\sigma_{x''z''}(x + dx/2)$ have non-canceling components in the x -direction while $\partial_x \sigma_{xx}$ contributes to the force normal to the bed.

publications by those authors, no explicit derivation of the curvature-related terms or justification of their omission are usually found in the literature. Hutter and coworkers introduced an explicit scaling analysis that shows which terms are of leading order if specific assumptions are made concerning the ratio of curvature radii to characteristic flow dimensions. Note, however, that the assumptions made by [3] leave only the centrifugal force due to curvature and velocity in the direction of the thalweg whereas the present treatment also includes effects of the lateral movement. Indeed, if x is the main flow direction, $u^y \ll u^x$ is often compensated by $\kappa_y \gg \kappa_x$ in channeled flows.

4.3 Evaluation of geometric weight factors

The equations (51) and (52) are esthetically pleasing and highlight the conservation properties that are important for shock-capturing numerical schemes. However, use of covariant velocity and stress components makes physical interpretation of the results of a calculation cumbersome, and particularly Eq. (49) is not well suited for numerical implementation. We revert therefore to physical components u^i and σ^{ij} and abandon the requirement that the averaged fields $\hat{\rho}$, \hat{u}^i and $\hat{\sigma}^{ij}$ appearing in the equations must rep-

resent *weighted* averages. They merely represent reference values that allow us to obtain the local field values with the help of the respective profile functions. If the normalization conditions $\int_0^1 f_\rho(\zeta)d\zeta = \int_0^1 f_\sigma(\zeta)d\zeta = 1$ are maintained, $\hat{\rho}$ and $\hat{\sigma}^{ij}$ will be close to the weighted averages where bed curvature is small. The same condition may be imposed on $f_u(\zeta)$, but if the density profile is not uniform, Favre averaging with $\int_0^1 f_\rho(\zeta)f_u(\zeta)d\zeta = 1$ may be considered instead.

In such a framework the depth-integrated mass balance, Eq. (46), and an analogous equation for momentum can be cast into the form

$$\partial_t (d_1 \sqrt{g_b} h \hat{\rho}) + \partial_\alpha (d_2^{(\alpha)} \sqrt{g_b} h \hat{\rho} \hat{u}^\alpha) = \sqrt{g_b} q_e, \quad (59)$$

$$\begin{aligned} & \partial_t (d_2^{(i)} \sqrt{g_b} h \hat{\rho} \hat{u}^i) + \partial_\alpha [\sqrt{g_b} h (d_3^{(i\alpha)} \hat{\rho} \hat{u}^i \hat{u}^\alpha - d_4^{(i\alpha)} \hat{\sigma}^{i\alpha})] \\ &= d_5^{(i)} \sqrt{g_b} h \hat{\rho} G^i - \sqrt{g_b} h (C_{jk}^i \hat{\rho} \hat{u}^j \hat{u}^k - D_{jk}^i \hat{\sigma}^{jk}) \\ & \quad - d_6^{(i)} \sqrt{g_b} \hat{\sigma}^{iz} + \sqrt{g_b} (d_7^{(i)} \hat{\sigma}^{iz} - d_8^{(i\alpha)} \hat{\sigma}^{i\alpha} \partial_\alpha h). \end{aligned} \quad (60)$$

If a metric of the form (38) is assumed, the coefficients d_1, \dots, d_8 and C_{jk}^i, D_{jk}^i are found to be

$$d_1 = \int_0^1 (1 - \kappa_x h \zeta)(1 - \kappa_y h \zeta) f_\rho(\zeta) d\zeta, \quad (61)$$

$$\begin{pmatrix} d_2^{(x)} \\ d_2^{(y)} \end{pmatrix} = \int_0^1 \begin{pmatrix} \frac{1 - \kappa_y h \zeta}{\sqrt{g_{xx}^{(b)}}} \\ \frac{1 - \kappa_x h \zeta}{\sqrt{g_{yy}^{(b)}}} \end{pmatrix} f_\rho(\zeta) f_u(\zeta) d\zeta, \quad (62)$$

$$\begin{pmatrix} d_3^{(xx)} \\ d_3^{(xy)} \\ d_3^{(yy)} \end{pmatrix} = \int_0^1 \begin{pmatrix} \frac{1 - \kappa_y h \zeta}{1 - \kappa_x h \zeta} \frac{1}{g_{xx}^{(b)}} \\ 1/\sqrt{g_b} \\ \frac{1 - \kappa_x h \zeta}{1 - \kappa_y h \zeta} \frac{1}{g_{yy}^{(b)}} \end{pmatrix} f_\rho(\zeta) f_u^2(\zeta) d\zeta, \quad (63)$$

$$\begin{pmatrix} d_4^{(xx)} \\ d_4^{(xy)} \\ d_4^{(yy)} \end{pmatrix} = \int_0^1 \begin{pmatrix} \frac{1-\kappa_y h \zeta}{1-\kappa_x h \zeta} \frac{1}{g_{xx}^{(b)}} \\ 1/\sqrt{g_b} \\ \frac{1-\kappa_x h \zeta}{1-\kappa_y h \zeta} \frac{1}{g_{yy}^{(b)}} \end{pmatrix} f_\sigma(\zeta) d\zeta, \quad (64)$$

$$\begin{pmatrix} d_5^{(x)} \\ d_5^{(y)} \end{pmatrix} = \int_0^1 \begin{pmatrix} \frac{1-\kappa_y h \zeta}{\sqrt{g_{xx}^{(b)}}} \\ \frac{1-\kappa_x h \zeta}{\sqrt{g_{yy}^{(b)}}} \end{pmatrix} f_\rho(\zeta) d\zeta, \quad (65)$$

$$\begin{pmatrix} d_6^{(x)} \\ d_6^{(y)} \end{pmatrix} = \begin{pmatrix} 1/\sqrt{g_{xx}^{(b)}} \\ 1/\sqrt{g_{yy}^{(b)}} \end{pmatrix} f_\sigma(0), \quad (66)$$

$$\begin{pmatrix} d_7^{(x)} \\ d_7^{(y)} \end{pmatrix} = \begin{pmatrix} \frac{1-\kappa_y h}{\sqrt{g_{xx}^{(b)}}} \\ \frac{1-\kappa_x h}{\sqrt{g_{yy}^{(b)}}} \end{pmatrix} f_\sigma(1), \quad (67)$$

$$\begin{pmatrix} d_8^{(xx)} \\ d_8^{(xy)} \\ d_8^{(yy)} \end{pmatrix} = \begin{pmatrix} \frac{1-\kappa_y h}{1-\kappa_x h} \frac{1}{g_{xx}^{(b)}} \\ 1/\sqrt{g_b} \\ \frac{1-\kappa_x h}{1-\kappa_y h} \frac{1}{g_{yy}^{(b)}} \end{pmatrix} f_\sigma(1), \quad (68)$$

$$\begin{pmatrix} C_{xx}^i \\ C_{xy}^i \\ C_{yy}^i \end{pmatrix} = \int_0^1 \begin{pmatrix} \frac{1-\kappa_y h \zeta}{1-\kappa_x h \zeta} \frac{\Gamma_{xx}^i(\zeta)}{g_{xx}^{(b)}} \\ \Gamma_{xy}^i(\zeta)/\sqrt{g_b} \\ \frac{1-\kappa_x h \zeta}{1-\kappa_y h \zeta} \frac{\Gamma_{yy}^i(\zeta)}{g_{yy}^{(b)}} \end{pmatrix} f_\rho(\zeta) f_u^2(\zeta) d\zeta \quad (69)$$

$$\begin{pmatrix} D_{xx}^i \\ D_{xy}^i \\ D_{yy}^i \end{pmatrix} = \int_0^1 \begin{pmatrix} \frac{1-\kappa_y h \zeta}{1-\kappa_x h \zeta} \frac{\Gamma_{xx}^i(\zeta)}{g_{xx}^{(b)}} \\ \Gamma_{xy}^i(\zeta)/\sqrt{g_b} \\ \frac{1-\kappa_x h \zeta}{1-\kappa_y h \zeta} \frac{\Gamma_{yy}^i(\zeta)}{g_{yy}^{(b)}} \end{pmatrix} f_\sigma(\zeta) d\zeta \quad (70)$$

These are 24 expressions—17 of which are integrals—that have to be evaluated once for each timestep and computational grid point. For the computer code to be practically usable, the integrals must allow closed-form evaluation, preferably in terms of polynomials that can be computed very efficiently. This is essentially the case if curvature-line coordi-

nates are used and the profile functions are polynomials, see the expressions listed in the Appendix B. (Integrands containing denominators $1 - \kappa_{x,y}h\zeta$ lead to logarithmic terms that may be approximated by the first few terms of a Taylor series thanks to $\kappa_{x,y}h \ll 1$.) All coefficients $d_1, \dots, d_8, C_{jk}^i, D_{jk}^i$ are thus expressible as polynomials in the flow depth h with spatially varying but time-independent coefficients that can be computed and stored before the time evolution of the system is computed.

An additional complication is implied by the curvilinear coordinates: Solving the balance equations does not immediately give the time evolution of the flow depth, but of the quantity $d_1(h)h$ (assuming fixed density for simplicity here), which is a non-linear function of h . However, thanks to the stipulated smallness of $\kappa_{x,y}h$, $d_1(h)h$ can be solved for h in a few simple iterations. (This problem does not occur in the coordinate system with uniform z -direction, see Appendix A.)

5 Constitutive equations in curvilinear coordinates

Formulating the constitutive equations in curvilinear coordinates is in many cases more than just a mathematical task because many of the currently popular models for GMFs do not completely specify material behavior. Often, only the shear stress is prescribed in terms of dynamical variables while e.g. hydrostatic pressure distribution is assumed for the normal stresses. When differential expressions in Cartesian coordinates relating normal stresses at neighboring points are transformed to curvilinear coordinates, they couple shear stresses to normal stresses. Therefore a consistent rheological formulation of the entire stress tensor must be given. The aim of the following brief discussions, mainly taken from [6, 7], is not completeness but to give a glimpse of the issues involved.

5.1 Newtonian fluids

The relation valid in Cartesian coordinates is

$$\sigma_{ij} = -p\delta_{ij} + \mu' D_{kk}\delta_{ij} + 2\mu \left(D_{ij} - \frac{1}{3} D_{kk}\delta_{ij} \right),$$

where p is the pressure, μ the (shear) viscosity, μ' the bulk viscosity connected to volume changes, and the symmetric part of the deformation rate tensor is defined as

$$D_{ij} \equiv \frac{1}{2}(\partial_j u_i + \partial_i u_j).$$

It is easily adapted to curvilinear coordinates,

$$\check{\sigma}^{ij} = -p g^{ij} + \mu' \check{D}_k{}^k g^{ij} + 2\mu \left(\check{D}^{ij} - \frac{1}{3} \check{D}_k{}^k g^{ij} \right), \quad (71)$$

if covariant derivatives are used in the expression for the deformation rate:

$$\begin{aligned} \check{D}_{ij} &= \frac{1}{2} \left(\mathcal{D}_j(g_{ik} \check{u}^k) + \mathcal{D}_i(g_{jk} \check{u}^k) \right) \\ &= \frac{1}{2} (g_{ik} \mathcal{D}_j + g_{jk} \mathcal{D}_i) \check{u}^k. \end{aligned} \quad (72)$$

We used the fact that the covariant derivative of the metric tensor vanishes in any coordinate system if the space is Euclidean (in our case, it is E^3). Note that covariant components of the velocity are used in (72), not physical ones.

5.2 Visco-plastic fluids – the Bingham rheology

Models based on the Bingham rheology like BING [8] specify the relationship between the shear rate $\partial_z u$ and the downslope shear stress τ by

$$\begin{cases} \partial_z u = 0 & \text{if } |\tau| < \tau_y \\ \tau = \text{sgn}(\partial_z u) \tau_y + \mu_B \partial_z u & \text{otherwise} \end{cases} \quad (73)$$

and assume hydrostatic longitudinal (and lateral) stresses. τ_y is the yield strength below which the material behaves as a solid, μ_B is the (Bingham) viscosity. If the von Mises failure criterion, stating that the material yields if the deviatoric stress exceeds a critical

value, is applied (73) can be generalized to

$$\begin{cases} \check{D}^{ij} = 0 & \text{if } \sqrt{I_2(\check{\sigma})} < \tau_y \\ \check{\sigma}^{ij} = \tau_y \frac{\check{D}^{ij}}{\sqrt{I_2(\check{D})}} + 2\mu_B \check{D}^{ij} & \text{otherwise} \end{cases} \quad (74)$$

where the second invariant of a second-rank tensor T^{ij} is given by

$$I_2(\check{T}) \equiv \frac{1}{2} \left(\text{Tr}(T^2) - \frac{1}{3}(\text{Tr}T)^2 \right). \quad (75)$$

See [6, Chap. 7] for a discussion and references to the original papers.

5.3 Dry friction – the Mohr–Coulomb yield criterion

A completely satisfactory extension of the simple Mohr–Coulomb yield criterion for plane shear,

$$\tau = \sigma_n \tan \phi, \quad (76)$$

with τ and σ_n the shear and normal stresses, respectively, and ϕ the friction angle, has not been found. If the plastic flow rule satisfies the coaxiality principle stating that the deformation rate tensor has the same principal axes as the excess shear stress tensor, unlimited dilation of the material is predicted if shear stress exceeding the limit given by (76) is applied (see [7] for a brief discussion). Arguments have been given [9] why coaxiality should not hold in sheared granular materials, but the resulting theory cannot be formulated in terms of tensor invariants in three dimensions.

If one is willing to accept one or the other of these shortcomings, one of the simplest invariant formulations uses the mean stress, $I_1(\sigma)/3 = \text{Tr} \sigma/3$, and the deviatoric part of the deformation rate, $\check{D}^{ij} \equiv \check{D}^{ij} - g^{ij} I_1(\check{D})/3$, and analogously for the stress tensor:

$$\begin{cases} \check{D}^{ij} = 0 & \text{if } I_2(\check{\sigma}) < \frac{1}{3} I_1(\check{\sigma}) \tan \phi \\ \check{\sigma}^{ij} = \frac{1}{3} I_1(\check{\sigma}) \tan \phi \frac{\check{D}^{ij}}{\sqrt{I_2(\check{D})}} & \text{otherwise.} \end{cases} \quad (77)$$

5.4 Granular fluids with dispersive pressure

[10] presented an extension of the Norem–Irgens–Schieldrop model [11], which in turn combines the Criminale–Ericksen–Filbey rheology with Mohr–Coulomb plastic behavior including cohesion. While the model shares the difficulties of the Mohr–Coulomb yield criterion mentioned above, it provides a simple way of incorporating the effect of intergranular collisions that may lead to fluidization of the flow. Irgens’ constitutive laws are manifestly invariant under rotations and can be easily modified to become invariant under general coordinate transformations:

$$\begin{aligned}
\check{\sigma}^{ij} = & -(p_u + p_e)g^{ij} + 2(\tau_y + p_e \tan \phi)\dot{\gamma}^{-1}\check{D}^{ij} \\
& + 2\rho\mu\dot{\gamma}^{n-1}\check{D}^{ij} + \rho(2\mu_1 - 4\mu_2)\dot{\gamma}^{n-2}\check{D}_k^i\check{D}^{kj} \\
& - \rho\mu_1\dot{\gamma}^{n-2}(\check{D}^{ij} - \check{W}_k^i\check{D}^{kj} + \check{D}_k^i\check{W}^{kj}) - \rho\mu_3\dot{\gamma}^n g^{ij}.
\end{aligned} \tag{78}$$

p_u and p_e are the pore and effective pressures, respectively. The latter is the negative stress transmitted across the granular skeleton; $p_e = 0$ indicates the transition between the dense (quasi-static/frictional) and the partially or fully fluidized (collisional/grain-inertia) flow regimes. The measure of shear is defined by $\dot{\gamma} = \sqrt{8I_2(\check{D})}$. The exponent n takes the value 2 for “classical” granular flows. Besides the deformation rate tensor, the vorticity tensor is also needed. Because of the anti-symmetry of \check{W}^{ij} and the symmetry of Γ_{jk}^i in j, k , the connection terms cancel:

$$\check{W}_{ij} \equiv \frac{1}{2}(\mathcal{D}_j\check{u}_i - \mathcal{D}_i\check{u}_j) = \frac{1}{2}(\partial_j\check{u}_i - \partial_i\check{u}_j). \tag{79}$$

6 Discussion

We briefly compare our approach and results with recent or parallel work that also aimed at formulating gravity mass flows on general surfaces, and attempt to estimate the order of magnitude of the curvature effects that are revealed by our geometric analysis.

6.1 Comparison with similar work

As far as we are aware, all models that include geometric effects beyond centrifugal forces are concerned with extending the Savage–Hutter model or a variant thereof, but much of the formalism can be carried over to other constitutive equations once the latter have been formulated in a coordinate-independent way, as discussed in Sect. 5.

[12] base their work on a reference surface that captures the curvature in the longitudinal direction only, and superpose a shallow, more detailed bed surface model over it, neglecting its curvature. Their model is therefore in principle restricted to mildly curved open slopes. They apply differential geometry and tensor calculus in a similar way as the present paper. In order to treat flows in gullies, [13] use a so-called master curve, which can be viewed as the curved centerline of a generalized surface of revolution, with the thalweg as generatrix. Again the detailed topography is modeled by means of a superposed surface function. Ordering assumptions for the curvatures and velocities derived from a scaling analysis suppress all curvature effects in the resulting equations except for centrifugal effects due to the thalweg curvature. They appear questionable, however, in narrow gullies where the transverse curvature often is an order of magnitude larger than the longitudinal one. Difficulties are expected to arise in the transition from a gully to an alluvial fan where the transverse curvature changes sign.

A number of authors have chosen to work with the bed surface directly. [14] use an Earth-oriented Cartesian X - Y - Z system. The usual hydrostatic assumption for the vertical Z -direction is not justified and vertical acceleration has to be taken into account; this corresponds to the centrifugal force terms in bed-surface-fitted coordinates (BSFC). Their method has the advantage of avoiding the conceptual and computational effort connected with the use of BSFC, but is at a disadvantage at very steep slopes and abrupt slope-angle changes. In contrast, [15]^{d)} start their analysis using techniques of tensorial calculus and differential geometry similar to ours. However, when deriving the stress tensor according to the Mohr–Coulomb failure criterion, they switch to a Cartesian coordinate system ori-

^{d)}The author thanks K. Hutter for drawing the papers [15, 16] to his attention, and I. Luca and Y.-C. Tai for sending him a preprint of their paper “Non-Cartesian, topography based boundary layer equations and approximations of gravity driven flows of ideal and viscous fluids”, submitted to *Math. Mod. Meth. Appl. Sci.*.

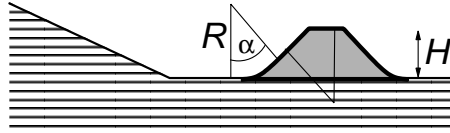


Figure 3: Schematic representation of a stopping dam for snow avalanches, indicating the relevant variables mentioned in the text.

ented along the instantaneous local flow direction to approximate plane shear flow in the x - z -plane. The stress tensor is then transformed to the Earth-oriented Cartesian system and the equations of motion are finally written in non-conservative form in that system. As in the original implementation of the Savage–Hutter model, their Lagrangean scheme experiences stability problems where shocks form.

[16] were the first to treat BSFC on a general curved surface, even though they often refer back to the velocity components in an Earth-oriented Cartesian system. As they do not avail themselves of the notational elegance of tensor calculus and do not explicitly mention the metric tensor, equivalent formulations in terms of contravariant vs. covariant components are derived with considerable effort. They treat a number of different approximations and show how the Navier–Stokes equations for low viscosity result in a model of the Savage–Hutter type if Coulomb bed friction is assumed. Their results are reproduced in the mentioned preprint by Luca and Tai, who use more transparent notation from differential geometry and tensor calculus and consider more general power-law velocity profiles. They do not, however, treat issues of practical implementation.

6.2 Order-of-magnitude estimates of curvature effects

The most important curvature effect is the increase or decrease of the frictional shear stress due to centrifugal forces experienced by a mass flowing along a curved trajectory. As a practically relevant example we consider snow avalanches flowing over a 16 m high dam at the avalanche test site Ryggfonn in Norway [17], see Fig. 3. It is easy to show that the dam has no effect on the runout distance of a mass subjected only to Coulombian dry friction forces with friction coefficient μ if centrifugal effects are neglected. The latter increase friction in the bends at the foot of the dam and reduce it at the crown. The velocity being higher at the foot, the net effect is enhanced friction. If we assume all

deflection angles to be equal ($\alpha \approx 40^\circ$), the loss of specific kinetic energy across the dam can be estimated as

$$\Delta E \approx 4\mu gh\alpha(1 - \mu\alpha - 2\mu^2\alpha^2) \approx (2 \dots 3)\mu gh \quad (80)$$

and shortens the runout distance of the avalanche by 2–3 dam heights, i. e., by 30–50 m in this case.

At abrupt slope changes with curvature κ , the shape of slices perpendicular to the flow direction deviates significantly from prismatic (see Fig. 2). Accordingly, for a given mass in a cell the actual flow height h_κ differs from h_0 , the one obtained for a cell without curvature, by a factor $h_\kappa/h_0 \approx 1 + \frac{1}{2}\kappa h_0$. In a tortuous, narrow channel with comparable curvature also in the transverse direction this factor may in rare cases lie outside the range [0.9, 1.1]. The increased or decreased flow height in the bends will locally increase or decrease the dry friction and the earth pressure gradient and so influence the flow dynamics to some degree. However, in most applications this effect can safely be neglected because the centrifugal effects on the friction are much stronger. The correction to the flow height also influences the mean velocity in the slice and thus indirectly the centrifugal effects, but this is masked by the deviation of the velocity profile in the bend from its assumed equilibrium shape, which is not accounted for in depth-averaged models.

Another effect of curvature is indicated in Fig. 2: Longitudinal and shear stresses at the cell boundaries contribute to the bed-normal stress and the longitudinal force on the cell, respectively. The appropriate scale for the stresses being ρgh , the resulting forces per unit mass are of the order of κgh , i. e., typically 0.1 g or less. Again, they may be safely neglected in many cases of practical interest, but it may be advisable to include them in very rugged topography as this can be achieved with moderate effort.

7 Conclusions

The main result of the present investigation is that the effects of complicated bed topography can be included in a consistent and transparent fashion in depth-averaged GMF

models if methods of classical differential geometry are applied. It is not necessary to require the curvature radii of the bed surface to be much larger than the length of the flow—it is sufficient for them to be significantly larger than the flow depth. One of the physical effects following naturally from the geometric formulation is the centrifugal force that has been included in a few of the previously published models; it can be practically important in sharp bends or in flows over obstacles through extra friction generated by an increased bed-normal stress.

The price to pay for enhanced applicability and accuracy of the models is a host of new terms involving the metric tensor and the connection coefficients derived from it. However, we have shown how to maintain a conservation formulation and to minimize the effort needed in computing the geometric coefficients appearing in flux and source terms. Even though they are time-dependent, evaluation of simple polynomials of the flow depth (with coefficients computed in the preprocessing phase) is sufficient.

There is a wide choice of coordinate systems, with their specific advantages and disadvantages with respect to the number of geometric terms in the equations and the complexity of mesh generation. Practical considerations will favor specific choices, and recommendations can be made once wide experience from real-world applications has been gained.

Acknowledgements

This research was financed by the European Union through the FP 5 project SATSIE (Avalanche Studies and Model Validation in Europe, EVG1-CT-2002-00059), the Norwegian Research Council through the research program SIP-8 “Offshore Geohazards”, and the ESF Integrated Project EUROMARGINS. Additional funding came from the Swiss National Science Foundation grant no. 200021-101911. I wish to thank Kolumban Hutter and Fridtjov Irgens for discussions related to topographic effects in avalanche models and Margarita Eglit for her most valuable comments on an early draft.

A Connection coefficients and geometric weight factors in a coordinate system with parallel z -coordinate lines

If the bed topography is given by a digital terrain model consisting of altitude values over a quadratic grid, the simplest coordinate system to construct projects the X and Y coordinate lines of the three-dimensional Cartesian system onto the bed surface and takes the z -coordinate parallel to the Z -coordinate, with uniform spacing. The corresponding metric is given in Eq. (30). For ease of notation, we set $p \equiv \tan \theta_x$, $q \equiv \tan \theta_y$ and $\Omega \equiv \partial_y p - \partial_x q$ in the following. The z -independence of the metric propagates to the connection coefficients and makes 9 out of 27 vanish. Calculating the coefficients d_1, \dots, d_8 and C_{jk}^i, D_{jk}^i becomes very simple because all geometrical factors can be taken outside the integrals.

Using the contravariant metric tensor

$$(g^{ij}(x, y)) = \begin{pmatrix} 1 & 0 & -p \\ 0 & 1 & -q \\ -p & -q & 1 + p^2 + q^2 \end{pmatrix}, \quad (81)$$

the connection coefficients listed in Eq. (82) are obtained. The weight factors in the mass and momentum balance equations are collected in Table 2.

Table 1: Connection coefficients for coordinate system with uniform z -direction.

$$\begin{aligned}
\Gamma_{11}^1 = \Gamma_{13}^1 &= \Gamma_{31}^1 = \Gamma_{33}^1 = \Gamma_{22}^2 = \Gamma_{23}^2 = \Gamma_{32}^2 = \Gamma_{33}^2 = \Gamma_{33}^3 = 0 \\
\Gamma_{12}^1 = \Gamma_{21}^1 &= \frac{1}{2}p\Omega \\
\Gamma_{22}^1 &= q\Omega \\
\Gamma_{23}^1 = \Gamma_{32}^1 &= \frac{1}{2}\Omega \\
\Gamma_{11}^2 &= -p\Omega \\
\Gamma_{12}^2 = \Gamma_{21}^2 &= -\frac{1}{2}q\Omega \\
\Gamma_{13}^2 = \Gamma_{31}^2 &= -\frac{1}{2}\Omega \\
\Gamma_{11}^3 &= \partial_x p + pq\Omega \\
\Gamma_{12}^3 = \Gamma_{21}^3 &= \frac{1}{2}(1 - p^2 + q^2)\partial_y p + \frac{1}{2}(1 + p^2 - q^2)\partial_x q \\
\Gamma_{13}^3 = \Gamma_{31}^3 &= \frac{1}{2}q\Omega \\
\Gamma_{22}^3 &= \partial_y q - pq\Omega \\
\Gamma_{23}^3 = \Gamma_{32}^3 &= -\frac{1}{2}p\Omega
\end{aligned} \tag{82}$$

Table 2: Geometry-dependent coefficients of flux and source terms for a coordinate system with uniform z -direction. The C_{jk}^i and D_{jk}^i are symmetric in the lower indices; coefficients with index combinations that cannot be obtained from those listed below by transposition of lower indices are zero.

$$\begin{aligned}
A &\equiv \sqrt{g_{xx}}, & B &\equiv \sqrt{g_{yy}}, & \sqrt{g} &= AB, \\
M &\equiv \int_0^1 f_\rho(\zeta) f_u(\zeta) d\zeta, & P &\equiv \int_0^1 f_\rho(\zeta) f_u^2(\zeta) d\zeta.
\end{aligned} \tag{83}$$

$$d_1 = 1 \tag{84}$$

$$d_2^x = M/A, \quad d_2^y = M/B \tag{85}$$

$$d_3^{xx} = P/A^2, \quad d_3^{xy} = P/(AB), \quad d_3^{yy} = P/B^2 \tag{86}$$

$$d_4^{xx} = 1/A^2, \quad d_4^{xy} = 1/(AB), \quad d_4^{yy} = 1/B^2 \tag{87}$$

$$d_5^x = 1/A, \quad d_5^y = 1/B \tag{88}$$

$$d_6^x = f_\sigma(0)/A, \quad d_6^y = f_\sigma(0)/B \tag{89}$$

$$d_7^x = f_\sigma(1)/A, \quad d_7^y = f_\sigma(1)/B \tag{90}$$

$$d_8^{xx} = \frac{f_\sigma(1)}{A^2}, \quad d_8^{xy} = \frac{f_\sigma(1)}{AB}, \quad d_8^{yy} = \frac{f_\sigma(1)}{B^2} \tag{91}$$

B Connection coefficients and geometric weight factors in a coordinate system of curvature lines

For reference, Eq. (92) lists the Christoffel symbols (connection coefficients) in the special curvilinear coordinate system that is given by the metric tensor (38). The z -lines are straight lines perpendicular to the bed surface ($z = 0$), and the scale is constant along them. The x and y coordinate lines at $z = 0$ are the directions of the two principal curvatures on the bed surface, $\kappa_{1,2}(x, y) = \kappa_{x,y}(x, y)$. The x , y and z lines are everywhere orthogonal to each other. As the covariant metric tensor g^{ij} is also diagonal, the general formula (22) specializes to $\Gamma_{jk}^i = \frac{1}{2}g^{(ii)}(\partial_j g_{ik} + \partial_k g_{ji} - \partial_i g_{jk})$ (no summation over i).

In the following we assume that the non-dimensionalized profile functions are the same for all components of the velocity vector and the stress tensor, respectively. Straightforward calculations lead to the results collected in Table 4; note that the right-hand sides are expressed in terms of physical components. Also, use is made of the normalization conditions for the profile functions. The resulting expressions are expanded in powers of $\kappa_x h$ or $\kappa_y h$ since these are assumed to be small quantities; in real-world situations, expansion up to the second power will be sufficient. In a similar way, the source terms containing connection coefficients are computed and expanded to second order in $\kappa_{x,y} h$, see Eqs. (103)–(112).

The decisive point is that all terms can be expressed through the averaged fields with geometric weight factors that may be approximated as polynomials of the flow depth with spatially varying but time-independent coefficients. These can be computed beforehand and stored in memory. In this way, the extra computational effort over models that neglect these curvature effects is moderate.

Table 3: Connection coefficients for coordinate system of curvature lines.

$$\begin{aligned}
\Gamma_{11}^1 &= \frac{1}{2}g^{11}(\partial_1 g_{11} + \partial_1 g_{11} - \partial_1 g_{11}) = \frac{1}{2}g^{11}\partial_1 g_{11} \\
&= \frac{\partial_x A}{A} - \frac{z \partial_x \kappa_x}{1 - \kappa_x z} \\
\Gamma_{12}^1 = \Gamma_{21}^1 &= \frac{1}{2}g^{11}(\partial_1 g_{21} + \partial_2 g_{11} - \partial_1 g_{12}) = \frac{1}{2}g^{11}\partial_2 g_{11} \\
&= \frac{\partial_y A}{A} - \frac{z \partial_y \kappa_x}{1 - \kappa_x z} \\
\Gamma_{13}^1 = \Gamma_{31}^1 &= \frac{1}{2}g^{11}(\partial_1 g_{13} + \partial_3 g_{11} - \partial_1 g_{13}) = \frac{1}{2}g^{11}\partial_3 g_{11} \\
&= -\frac{\kappa_x}{1 - \kappa_x z} \\
\Gamma_{22}^1 &= \frac{1}{2}g^{11}(\partial_2 g_{12} + \partial_2 g_{21} - \partial_1 g_{22}) = -\frac{1}{2}g^{11}\partial_1 g_{22} \\
&= \left(\frac{B(1 - \kappa_y z)}{A(1 - \kappa_x z)}\right)^2 \left(\frac{z \partial_x \kappa_y}{1 - \kappa_y z} - \frac{\partial_x B}{B}\right) \\
\Gamma_{23}^1 = \Gamma_{32}^1 &= \frac{1}{2}g^{11}(\partial_2 g_{13} + \partial_3 g_{21} - \partial_1 g_{23}) = 0 \\
\Gamma_{33}^1 &= \frac{1}{2}g^{11}(\partial_3 g_{13} + \partial_3 g_{31} - \partial_1 g_{33}) = 0 \\
\Gamma_{11}^2 &= \frac{1}{2}g^{22}(\partial_1 g_{21} + \partial_1 g_{12} - \partial_2 g_{11}) = -\frac{1}{2}g^{22}\partial_2 g_{11} \\
&= \left(\frac{A(1 - \kappa_x z)}{B(1 - \kappa_y z)}\right)^2 \left(\frac{z \partial_y \kappa_x}{1 - \kappa_x z} - \frac{\partial_y A}{A}\right) \\
\Gamma_{12}^2 = \Gamma_{21}^2 &= \frac{1}{2}g^{22}(\partial_1 g_{22} + \partial_2 g_{12} - \partial_2 g_{12}) = \frac{1}{2}g^{22}\partial_1 g_{22} \\
&= \frac{\partial_x B}{B} - \frac{z \partial_x \kappa_y}{1 - \kappa_y z} \\
\Gamma_{13}^2 = \Gamma_{31}^2 &= \frac{1}{2}g^{22}(\partial_1 g_{23} + \partial_3 g_{12} - \partial_2 g_{13}) = 0 \\
\Gamma_{22}^2 &= \frac{1}{2}g^{22}(\partial_2 g_{22} + \partial_2 g_{22} - \partial_2 g_{22}) = \frac{1}{2}g^{22}\partial_2 g_{22} \\
&= \frac{\partial_y B}{B} - \frac{z \partial_y \kappa_y}{1 - \kappa_y z} \\
\Gamma_{23}^2 = \Gamma_{32}^2 &= \frac{1}{2}g^{22}(\partial_2 g_{23} + \partial_3 g_{22} - \partial_2 g_{23}) = \frac{1}{2}g^{22}\partial_3 g_{22} \\
&= -\frac{\kappa_y}{1 - \kappa_y z} \\
\Gamma_{33}^2 &= \frac{1}{2}g^{22}(\partial_3 g_{23} + \partial_3 g_{32} - \partial_2 g_{33}) = 0
\end{aligned} \tag{92}$$

Table 3: (Continued from preceding page.)

$$\begin{aligned}
\Gamma_{11}^3 &= \frac{1}{2}g^{33}(\partial_1 g_{31} + \partial_1 g_{13} - \partial_3 g_{11}) = -\frac{1}{2}g^{33}\partial_3 g_{11} \\
&= A^2(1 - \kappa_x z)\kappa_x \\
\Gamma_{12}^3 = \Gamma_{21}^3 &= \frac{1}{2}g^{33}(\partial_1 g_{32} + \partial_2 g_{13} - \partial_3 g_{12}) = 0 \\
\Gamma_{13}^3 = \Gamma_{31}^3 &= \frac{1}{2}g^{33}(\partial_1 g_{33} + \partial_3 g_{13} - \partial_3 g_{13}) = 0 \\
\Gamma_{22}^3 &= \frac{1}{2}g^{33}(\partial_2 g_{32} + \partial_2 g_{23} - \partial_3 g_{22}) = -\frac{1}{2}g^{33}\partial_3 g_{22} \\
&= B^2(1 - \kappa_y z)\kappa_y \\
\Gamma_{23}^3 = \Gamma_{32}^3 &= \frac{1}{2}g^{33}(\partial_2 g_{33} + \partial_3 g_{23} - \partial_3 g_{23}) = 0 \\
\Gamma_{33}^3 &= \frac{1}{2}g^{33}(\partial_3 g_{33} + \partial_3 g_{33} - \partial_3 g_{33}) = 0
\end{aligned} \tag{93}$$

Table 4: Geometry-dependent flux and source terms. The C_{jk}^i and D_{jk}^i are symmetric in the lower indices; coefficients with index combinations that cannot be obtained from those listed below by transposition of lower indices are zero. Signs of approximate equality indicate that the Taylor series was truncated after the quadratic term in $\kappa_x h$ or $\kappa_y h$.

$$\begin{aligned}
r &\equiv \frac{1}{s} \equiv \kappa_y / \kappa_x, & A &\equiv \sqrt{g_{xx}^{(b)}}, & B &\equiv \sqrt{g_{yy}^{(b)}}, & \sqrt{g_b} &= AB, \\
\begin{pmatrix} I \\ J \end{pmatrix} &\equiv \int_0^1 f_\rho(\zeta) \begin{pmatrix} \zeta \\ \zeta^2 \end{pmatrix} dz, & \begin{pmatrix} M \\ N \end{pmatrix} &\equiv \int_0^1 f_\rho(\zeta) f_u(\zeta) \begin{pmatrix} 1 \\ \zeta \end{pmatrix} d\zeta, \\
\begin{pmatrix} P \\ Q \\ R \end{pmatrix} &\equiv \int_0^1 f_\rho(\zeta) f_u^2(\zeta) \begin{pmatrix} 1 \\ \zeta \\ \zeta^2 \end{pmatrix} d\zeta, & \begin{pmatrix} T \\ U \end{pmatrix} &\equiv \int_0^1 f_\sigma(\zeta) \begin{pmatrix} \zeta \\ \zeta^2 \end{pmatrix} d\zeta.
\end{aligned} \tag{94}$$

$$d_1 = 1 - (\kappa_x + \kappa_y)hI + \kappa_x \kappa_y h^2 J \tag{95}$$

$$d_2^x = \frac{1}{A}(M - \kappa_y h N), \quad d_2^y = \frac{1}{B}(M - \kappa_x h N) \tag{96}$$

$$d_3^{xx} = \frac{1}{A}[P + \kappa_x h(1-r)Q + (\kappa_x h)^2(1-r)R], \quad d_3^{xy} = \frac{1}{\sqrt{g_b}}P,$$

$$d_3^{yy} = \frac{1}{B}[8P + \kappa_y h(1-s)Q + (\kappa_y h)^2(1-s)R] \tag{97}$$

$$d_4^{xx} = \frac{1}{A}[1 + \kappa_x h(1-r)T + (\kappa_x h)^2(1-r)U], \quad d_4^{xy} = \frac{1}{\sqrt{g_b}},$$

$$d_4^{yy} = \frac{1}{B}[1 + \kappa_y h(1-s)T + (\kappa_y h)^2(1-s)U] \tag{98}$$

$$d_5^x = \frac{1}{A}(1 - \kappa_y h I), \quad d_5^y = \frac{1}{B}(1 - \kappa_x h I) \tag{99}$$

$$d_6^x = \frac{1}{A}f_\sigma(0), \quad d_6^y = \frac{1}{B}f_\sigma(0) \tag{100}$$

$$d_7^x = \frac{1 - \kappa_y h}{A}f_\sigma(1), \quad d_7^y = \frac{1 - \kappa_x h}{B}f_\sigma(1) \tag{101}$$

$$d_8^{xx} = \frac{1}{A^2} \frac{1 - \kappa_y h}{1 - \kappa_x h} f_\sigma(1), \quad d_8^{xy} = \frac{1}{\sqrt{g_b}} f_\sigma(1), \quad d_8^{yy} = \frac{1}{B^2} \frac{1 - \kappa_x h}{1 - \kappa_y h} f_\sigma(1) \tag{102}$$

Table 4: (Continued from preceding page.)

$$\begin{pmatrix} C_{xx}^x \\ D_{xx}^x \end{pmatrix} = \frac{1}{A^2} \left[\begin{pmatrix} P \\ 1 \end{pmatrix} \frac{\partial_x A}{A} + \begin{pmatrix} Q \\ T \end{pmatrix} \left((1-r) \frac{\partial_x A}{A} - \frac{\partial_x \kappa_x}{\kappa_x} \right) \kappa_x h \right. \\ \left. + \begin{pmatrix} R \\ U \end{pmatrix} \left((1-r) \frac{\partial_x A}{A} - (2-r) \frac{\partial_x \kappa_x}{\kappa_x} \right) (\kappa_x h)^2 \right] \quad (103)$$

$$\begin{pmatrix} C_{xy}^x \\ D_{xy}^x \end{pmatrix} = \frac{1}{\sqrt{g_b}} \left[\begin{pmatrix} P \\ 1 \end{pmatrix} \frac{\partial_y A}{A} - \begin{pmatrix} Q \\ T \end{pmatrix} \frac{\partial_y \kappa_x}{\kappa_x} \kappa_x h - \begin{pmatrix} R \\ U \end{pmatrix} \frac{\partial_y \kappa_x}{\kappa_x} (\kappa_x h)^2 \right] \quad (104)$$

$$\begin{pmatrix} C_{xz}^x \\ D_{xz}^x \end{pmatrix} = -\frac{1}{A} \kappa_x \left[\begin{pmatrix} P \\ 1 \end{pmatrix} + \begin{pmatrix} Q \\ T \end{pmatrix} (1-r) \kappa_x h + \begin{pmatrix} R \\ U \end{pmatrix} (1-r) (\kappa_x h)^2 \right] \quad (105)$$

$$\begin{pmatrix} C_{yy}^x \\ D_{yy}^x \end{pmatrix} = -\frac{1}{A^2} \left[\begin{pmatrix} P \\ 1 \end{pmatrix} \frac{\partial_x B}{B} + \begin{pmatrix} Q \\ T \end{pmatrix} \left((1-r) \frac{\partial_x B}{B} - \frac{\partial_x \kappa_y}{\kappa_x} \right) \kappa_x h \right. \\ \left. + \begin{pmatrix} R \\ U \end{pmatrix} \left((1-r) \frac{\partial_x B}{B} - \frac{\partial_x \kappa_y}{\kappa_x} \right) (\kappa_x h)^2 \right] \quad (106)$$

$$\begin{pmatrix} C_{xx}^y \\ D_{xx}^y \end{pmatrix} = -\frac{1}{B^2} \left[\begin{pmatrix} P \\ 1 \end{pmatrix} \frac{\partial_y A}{A} + \begin{pmatrix} Q \\ T \end{pmatrix} \left((1-s) \frac{\partial_y A}{A} - \frac{\partial_y \kappa_x}{\kappa_y} \right) \kappa_y h \right. \\ \left. + \begin{pmatrix} R \\ U \end{pmatrix} \left((1-s) \frac{\partial_y A}{A} - \frac{\partial_y \kappa_x}{\kappa_y} \right) (\kappa_y h)^2 \right] \quad (107)$$

$$\begin{pmatrix} C_{xy}^y \\ D_{xy}^y \end{pmatrix} = \frac{1}{\sqrt{g_b}} \left[\begin{pmatrix} P \\ 1 \end{pmatrix} \frac{\partial_x B}{B} - \begin{pmatrix} Q \\ T \end{pmatrix} \frac{\partial_x \kappa_y}{\kappa_y} \kappa_y h - \begin{pmatrix} R \\ U \end{pmatrix} \frac{\partial_x \kappa_y}{\kappa_y} (\kappa_y h)^2 \right] \quad (108)$$

$$\begin{pmatrix} C_{yy}^y \\ D_{yy}^y \end{pmatrix} = \frac{1}{B^2} \left[\begin{pmatrix} P \\ 1 \end{pmatrix} \frac{\partial_y B}{B} + \begin{pmatrix} Q \\ T \end{pmatrix} \left((1-s) \frac{\partial_y B}{B} - \frac{\partial_y \kappa_y}{\kappa_y} \right) \kappa_y h \right. \\ \left. + \begin{pmatrix} R \\ U \end{pmatrix} \left((1-s) \frac{\partial_y B}{B} - (2-s) \frac{\partial_y \kappa_y}{\kappa_y} \right) (\kappa_y h)^2 \right] \quad (109)$$

$$\begin{pmatrix} C_{yz}^y \\ D_{yz}^y \end{pmatrix} = -\frac{1}{B} \kappa_x \left[\begin{pmatrix} P \\ 1 \end{pmatrix} + \begin{pmatrix} Q \\ T \end{pmatrix} (1-s) \kappa_y h + \begin{pmatrix} R \\ U \end{pmatrix} (1-s) (\kappa_y h)^2 \right] \quad (110)$$

$$\begin{pmatrix} C_{xx}^z \\ D_{xx}^z \end{pmatrix} = \kappa_x \left[\begin{pmatrix} P \\ 1 \end{pmatrix} - \begin{pmatrix} Q \\ T \end{pmatrix} \kappa_y h \right] \quad (111)$$

$$\begin{pmatrix} C_{yy}^z \\ D_{yy}^z \end{pmatrix} = \kappa_y \left[\begin{pmatrix} P \\ 1 \end{pmatrix} - \begin{pmatrix} Q \\ T \end{pmatrix} \kappa_x h \right] \quad (112)$$

References

- [1] E. M. Eglit. Some mathematical models of snow avalanches. In M. Shahinpoor, editor, *Advances in the Mechanics and the Flow of Granular Materials*, volume II, pages 577–588. Trans Tech Publications, Clausthal-Zellerfeld, Germany, 1st edition, 1983.
- [2] S. B. Savage and K. Hutter. The dynamics of avalanches of granular material from initiation to runout. Part I: Analysis. *Acta Mechanica*, 86:201–223, 1991.
- [3] S. P. Pudasaini, Y. Wang, and K. Hutter. Dynamics of avalanches along general mountain slopes. *Annals Glaciol.*, 38:357–362, 2004.
- [4] D. Issler, P. Gauer, and M. Barbolini. Continuum models of particle entrainment and deposition in snow drift and avalanche dynamics. In R. Balean, editor, *Models of Continuum Mechanics in Analysis and Engineering. Proceedings of a conference held at the Technische Universität Darmstadt, September 30 to October 2, 1998*, pages 58–80, Aachen – Maastricht, 2000. Shaker Verlag.
- [5] D. Issler and T. Jóhannesson. On the formulation of entrainment in gravity mass flow models. NGI Report 20021048–12, Norwegian Geotechnical Institute, N–0806 Oslo, Norway, 2006. To be submitted.
- [6] P. Coussot. *Mudflow Rheology and Dynamics*. IAHR Monograph Series. A. A. Balkema, Rotterdam, The Netherlands, 1997.
- [7] C. Ancey. Plasticity and geophysical flows: A review. *J. Non-Newtonian Fluid Mech.*, 142:4–35, 2007.
- [8] J. Imran, P. Harff, and G. Parker. A numerical model of submarine debris flows with graphical user interface. *Computers Geosci.*, 274(6):717–729, 2001.
- [9] G. Mandl and R. Fernández Luque. Fully developed plastic shear flow of granular materials. *Géotech.*, 20(3):277–307, 1970.

- [10] F. Irgens. Simplified simulation model of snow avalanches and landslides. Paper presented at 21st Intl. Congress of Theoretical and Applied Mechanics, Chicago, U.S.A., 27 Aug. to 2 Sept. 2000, 2000.
- [11] H. Norem, F. Irgens, and B. Schieldrop. A continuum model for calculating snow avalanche velocities. In B. Salm and H. Gubler, editors, *Avalanche Formation, Movement and Effects. Proceedings of the Davos Symposium, September 1986*, IAHS Publication No. 162, pages 363–380, Inst. of Hydrology, Wallingford, Oxfordshire OX10 8BB, UK, 1987. IAHS Press.
- [12] J. M. N. T. Gray, M. Wieland, and K. Hutter. Gravity-driven free surface flow of granular avalanches over complex basal topography. *Proc. R. Soc. Lond. A*, 455:1841–1874, 1999.
- [13] S. P. Pudasaini and K. Hutter. Rapid shear flows of dry granular masses down curved and twisted channels. *J. Fluid Mech.*, 495:192–208, 2003.
- [14] R. P. Denlinger and R. M. Iverson. Granular avalanches across irregular three-dimensional terrain: Theory and computation. *J. Geophys. Res.*, 109(F01014, doi:10.1029/2003JF000085):1–14, 2004.
- [15] S. De Toni and P. Scotton. Two-dimensional mathematical and numerical model for the dynamics of granular avalanches. *Cold Regions Sci. Technol.*, 43(1–2):36–48; doi:10.1016/j.coldregions.2005.05.002, 2005.
- [16] F. Bouchut and M. Westdickenberg. Gravity driven shallow water models for arbitrary topography. *Comm. Math. Sci.*, 2(3):359–389, 2004.
- [17] K. Lied, A. Moe, K. Kristensen, and D. Issler. Ryggfonn. Full scale avalanche test site and the effect of the catching dam. In M. Naaim and F. Naaim-Bouvet, editors, *Snow and avalanches test sites — Sites expérimentaux dédiés à l'étude de la neige et des avalanches. Proceedings of the International Seminar on Snow and Avalanches Test Sites in the Memory of Philippe Revol, Grenoble 22–23 novembre 2001*, pages 25–98, B.P. 44, F–92163 Antony cedex, France, 2004. Cemagref Editions.